TRANSFER REACTIONS WITH SOLENOIDAL SPECTROMETERS*

S.J. Freeman

Experimental Physics Department, CERN, Switzerland
and
University of Manchester, Manchester, UK

Received 9 November 2022, accepted 19 January 2023, published online 22 March 2023

The approach of studying direct reactions with solenoidal spectrometers is discussed with reference to transfer reactions, in particular, with a short review of existing solenoidal spectrometers.

DOI:10.5506/APhysPolBSupp.16.4-A19

1. Introduction

Reactions involving the transfer of nucleons between nuclei have been studied for many years and, where a direct mechanism dominates, they can be used as a probe of nuclear structure.

Although there were precursor ideas in the literature [1, 2], direct reaction processes were highlighted in two short back-to-back papers published in *Physical Review* in 1950 [3, 4]. The first of these (co-authored by Józef Rotblat, the British–Polish physicist who later won the Nobel Peace Prize) described a study of the $^{16}\mathrm{O}(d,p)^{17}\mathrm{O}$ reaction with an 8-MeV beam from the Liverpool cyclotron. This was the first publication to map out detailed angular distributions for protons populating the ground and first-excited states in ^{17}O over a wide angular range; attention was drawn to the forward peaks and that their shapes differed below 50°. Similar findings had also been observed at the same laboratory for the $^{27}\mathrm{Al}(d,p)$ reaction [5]. In the second paper, Butler proposed a direct stripping process, where one of the nucleons in the deuteron is absorbed by the target and "the other merely carries off the balance of energy and momentum". He was then able to reproduce the angular distributions which were characteristic of the orbital angular momentum transferred in the reaction [4].

* Presented at the Zakopane Conference on Nuclear Physics, *Extremes of the Nuclear Landscape*, Zakopane, Poland, 28 August–4 September, 2022.

Such a single-neutron transfer is only one example of a broad class of direct reactions [6–9], which also includes inelastic scattering and the transfer of pairs or clusters of nucleons. Direct reactions are characterised by a single-step mechanism to specific final states or resonances. The excitation of the residual nucleus proceeds via a single degree of freedom, such as the addition/removal of a single nucleon, the excitation of a single mode of vibration, or the transfer of a single composite unit of nucleons such as a pair or cluster. With only a single step, the reaction amplitude has an explicit dependency on initial and final states that can be exploited as a probe of nuclear structure. If one has a reasonably reliable model to describe the entrance and exit channels, overlap integrals can be extracted, albeit in a model-dependent way. For example, in transfer reactions, spectroscopic factors reflect the overlap between the final state and an independent-particle model wave function corresponding to the target nucleus plus/minus a transferred nucleon. This also means that direct reactions are very selective; transfer reactions populate strongly single-particle-like states, cluster transfer populate states that exhibit corresponding cluster structures, *etc.* As noted by Butler, the angular distributions are characteristic of the orbital angular momentum transfer ℓ and, if polarised beams are used, reactions are sensitive to the transferred total angular momentum.

Of course, a particular reaction can proceed by a non-direct mechanism. For example, the (d, p) reaction might involve several steps that distribute energy between several nucleons in the target before the emission of a proton; then the simple connection between initial and final states is lost. Therefore, experiments which aim to probe structure using extracted overlaps are normally performed under conditions that maximise the contribution of the direct process by measuring the outgoing light ion at forward centre-of-mass (CM) angles with beam energies of around 10 MeV/u.

Historically, measurements generally involved a light-ion beam on a heavy target, which was the subject of study; this arrangement is known as *normal kinematics*. Two experimental approaches were developed. One involved using magnetic fields to momentum analyse the outgoing ions and the excitation energy spectrum of the residual nucleus deduced by applying conservation laws to the two-body kinematics. Simple dipole magnets rapidly evolved into more complex spectrometers with ingenious aberration and kinematic corrections. Detection of the particles at the focal plane of these devices also developed from photographic emulsion, through delay line readout, to single-wire readout using integrated electronics. The other approach was to measure ion energies directly using a suitable detector; significant progress was made following the development of high-resolution silicon semiconductor devices. Large area, segmented Si detectors led to large improvements in acceptance, and complex composite arrays have been developed using Si in combination with other detector types.

More recently, the focus has switched to exotic isotopes, away from the line of β stability. This necessitates a change in approach as, for most radioactive isotopes, there is not time to manufacture a target before the nuclei decay and they must be used as a radioactive beam. Such a heavy beam on a light target, so-called *inverse kinematics*, presents significant experimental challenges.

Any measurements made in the laboratory must be transferred to the CM frame to reconstruct Q values or excitation energies for the residual nucleus. However, as shown in Fig. 1 (a), the laboratory energy of outgoing particles populating a particular state varies with angle. This variation is called *kinematic shift*, which is a limiting factor for the ion-energy resolution in a detector accepting a range of laboratory angles. Moreover, the variation in kinematic shift with angle is different for different ion energies. This is hardly noticeable in normal kinematics. In inverse kinematics, it leads to a severe compression when transforming to the Q-value spectrum at the forward CM angles where the direct yields are usually highest. This is seen in Fig. 1 (a) where the laboratory ion energies corresponding to different excited states get closer together as the laboratory angle increases.

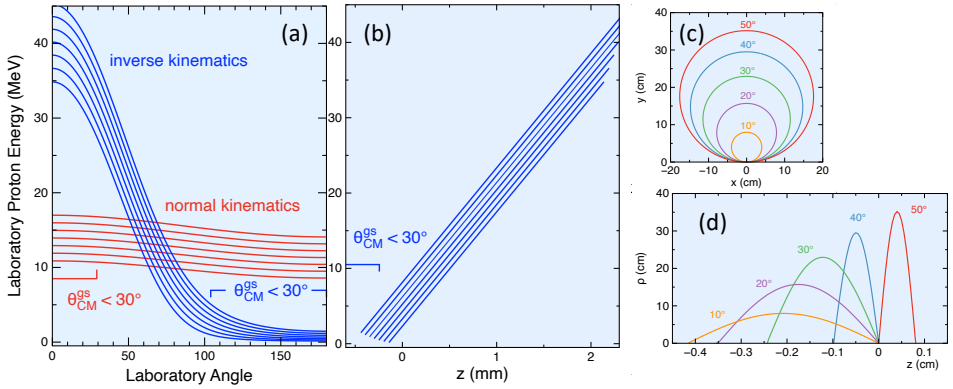

Fig. 1. Kinematic quantities for the ^{30}Mg(d,p) reaction at 8.52 MeV/u. (a) Energies of protons as a function of laboratory angle, calculated for a set of fictitious excited states from 0 to 6 MeV at 1 MeV spacing. Regions of forward CM angles are indicated. (b) Protons energies for the same states as a function of the position of return to an axis (z) in a solenoidal field of strength 2.5 T. (c) Proton trajectories in the x–y plane populating the ground state for different θ_{CM}. (d) Radii of those trajectories ρ as a function of z.

Both kinematic shift and compression affect the resolution that can be obtained in Q-value or excitation spectra. For inverse kinematics, the velocity of the CM is much higher than the corresponding reaction in normal kinematics, giving a greater kinematic shift and worse problems in terms of

resolution. Measurements of only ion energy/momenta at a fixed angle lead to poor Q-value resolutions in reactions with a heavy beam, often of several hundred keV, creating difficulty in resolving individual excited states.

One way to improve the situation is to measure, in coincidence with the outgoing ion, any γ rays emitted as the populated state decays using high-resolution detectors [10]. If the radiative decay scheme is known, or can be deduced, the excitation energy of the state can be reconstructed to within $\sim$ 10 keV. However, this method relies on the state having a reasonable radiative decay probability and a lifetime that is short compared to any limitations imposed by the measurement, such as flight time through a fiducial volume. Reactions populating ground states, unbound resonances, and isomers remain tricky.

2. The solenoidal method

In 1999, an alternative approach was suggested by Schiffer [11] and it is illustrated in Fig. 2. If the reaction is performed in a uniform magnetic

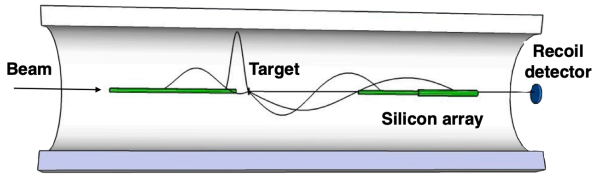

Fig. 2. A schematic diagram of a solenoidal spectrometer, where a uniform magnetic field is oriented along the beam direction. (Figure courtesy of B.P. Kay.)

field oriented along the beam axis, the emitted particles execute cyclotron motion in the plane perpendicular to the axis (see Fig. 1 (c)). Any parallel component of velocity will transport the particle up or down the beam axis (see Fig. 1 (d)). The combined motion is a helical orbit, which will spiral and eventually return to the axis at a position z from the target after a time equal to the cyclotron period, $T_{\rm cyc} = 2m\pi/Beq$. The device is therefore dispersive along the axis in terms of the parallel velocity component in the laboratory, depending on the field strength B and the charge-to-mass ratio qe/m of the ion. If a hollow position-sensitive array surrounds the beam axis, the position of return z and the laboratory energy of the particle $E_{\rm lab}$ can be measured. If the radial width of the on-axis detector is considered negligible, the CM energy of the particle $E_{\rm CM}$ is given by

$$E_{\rm CM} = E_{\rm lab} + \frac{m}{2}V_{\rm CM}^2 - \frac{mV_{\rm CM}}{T_{\rm cyc}}z\,,$$

and the angle in the CM by

$$\cos\theta_{\mathrm{CM}} = \frac{v_{\mathrm{lab}}^2 - V_{\mathrm{CM}}^2 - v_0^2}{2v_0 V_{\mathrm{CM}}} ,$$

where v_{lab} and v_0 are the ion velocity in the laboratory and CM, and V_{CM} is the velocity of the CM [12].

These equations embody the concept of the solenoidal spectrometer. For ions populating a particular excitation energy, those with different CM angles have different parallel components of laboratory velocity and return to the axis at different values of z (see Fig. 1 (d)). The expression above is linear in z, so laboratory and CM energies of the ions are related only by an additive offset. The linear relationship effectively eliminates the compression of excited states in conventional approaches since the spacing of excited states in the CM is the same as in the laboratory frame. On a plot of ion energy against position, different excited states, therefore, form simple straight-line loci, with different θ_{CM} along the line and a slope related to the velocity of the CM, the mass of the ion, and the cyclotron period, as shown in Fig. 1 (b). These lines are apparent in the experimental spectrum in Fig. 4 (a); the non-linearity or curling apparent at the low proton energies is an effect of the finite size of the array, whereas the expression above assumes a negligible array radius. This can be corrected during analysis.

An analogue of kinematic shift, $\mathrm{d}E/\mathrm{d}z$, does contribute to the resolution via the position resolution of the detector, however, this is small ($\sim$ 15–20 keV) for typical position resolutions ($\sim$ 1 mm). There are other contributions to the Q-value resolution, including detector energy resolution, beam spot size and energy spread, and energy-loss effects in the target. The latter usually dominate in the *ion-energy* resolution for high-Z beams, but the Q-value spectrum still benefits from the lack of compression.

A time-of-flight measurement, yielding the cyclotron period, can be useful to help identify the particle via qe/m. Alternatively, the reaction can be selected by identifying the heavy recoiling nucleus when needed, for example, if the beam has contaminants.

The acceptance depends on several geometric parameters and the field strength. The length of the on-axis array limits the range of angles of ions that will be detected. Ions emitted at certain angles will hit the wall of the solenoid and are lost before returning to an axis, so the magnet bore is an important parameter. Below a certain angle to the beam axis, ions will enter the hollow bore of the array and will not be detected. Trajectories that are emitted close to the plane of the target may be blocked by the thickness of the target frame or support. It is serendipitous that a good acceptance can be obtained by a solenoidal magnet of the similar strength and dimensions to those used in hospital MRI systems. Recycled medical imaging systems provided a cost-effective route of implementing all the existing solenoidal spectrometers.

It should be noted that ions at particular energies and angles may undertake multiple orbits within the solenoidal field before hitting the on-axis detector, complicating the interpretation of data. However, these are easily identified by measurements of $T_{\rm cyc}$, or can be removed by a suitable on-axis blocker at the position of their first return. An example of double turns can be seen in the counts in the region of $z > -200$ cm in Fig. 4 (a) superimposed on the main kinematic lines.

More details on the solenoidal method can be found in Ref. [12].

3. Solenoidal spectrometers

Three solenoidal spectrometers have been developed: HELIOS, ISS, and SOLARIS as shown in Fig. 3. Although similar in approach, they receive very different types of beam, making their individual science programmes unique.

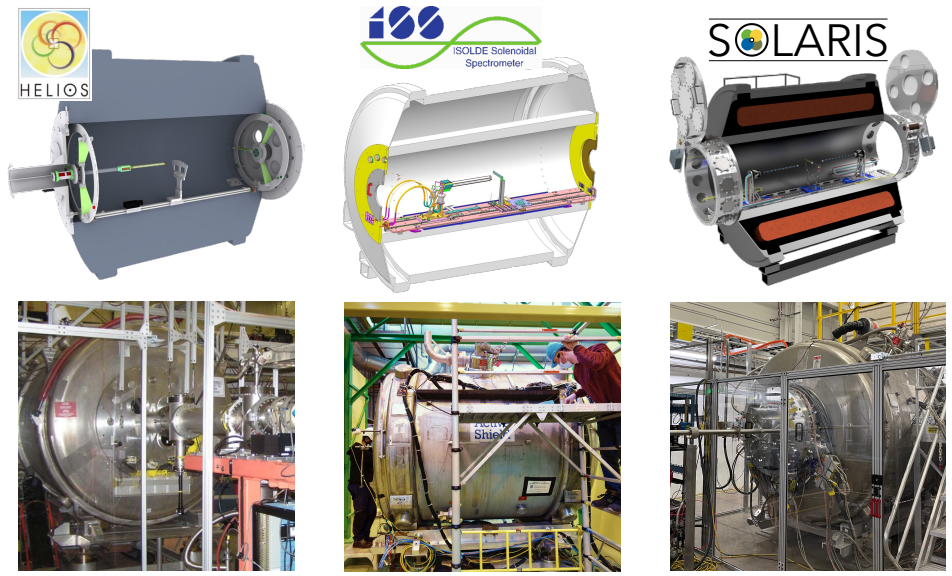

Fig. 3. The existing solenoidal spectrometers (ISS ©CERN, HELIOS courtesy of B. Digiovine, and SOLARIS courtesy of B.P. Kay).

3.1. HELIOS — the Helical Orbit Spectrometer at Argonne

HELIOS has been in operation at the Argonne National Laboratory since 2008 [13]. A 2.85-T magnet is used with stable beams, in-flight radioactive beams, and accelerated fission fragments. The on-axis array is composed of resistive-division position-sensitive silicon detectors operated in coincidence with several recoil detectors, which include annular silicon arrays and

a high-rate ionisation chamber. Polyethylene, deuterated polyethylene, tritiated titanium, LiF, and cryogenic helium gas cells have been used as targets. Beam current and target thickness are monitored with a sectored Si luminosity detector measuring elastically scattered particles from the target. Different arrangements of these detectors are used to measure reactions where the particular kinematics result in the higher yield at forward CM angles appearing at backward laboratory angles — such as (d, p) and (t, p) — and reactions where the maxima of the angular distribution are forward in the laboratory — such as (d, α), (d, h), and (p, p'). Q-value resolutions as low as 80 keV have been achieved.

With fifteen years of productive running, it is difficult to summarise the scientific output of HELIOS within the space available, so readers are directed to the extensive list of publications [14]. A recent highlight was a study probing the quenching of single-particle strength [15]. This study took advantage of a natural cocktail beam of ^{14}N and ^{14}C to induce (d, p) reactions simultaneously on both isotopes. The $A = 15$ residual systems span a large range in ΔS, the difference in neutron and proton separation energies. ΔS is — 20 MeV for ^{14}C+n and +8 MeV for ^{14}N+n. Relative spectroscopic factors for $1s_{1/2}$ and $0d_{5/2}$ orbitals were deduced without many of the usual systematic uncertainties due to the simultaneous measurement. In *both* systems, spectroscopic factors were reduced by a factor of ~ 0.5 compared to the independent-particle model and by a factor of ~ 0.6 compared to the shell-model calculations. This is in distinct contrast to the results of intermediate energy knockout from ^{9}Be and ^{12}C targets, where a strong variation in reduction factors with ΔS has been observed [16]. These findings add to the growing evidence for a disparity between heavy-ion knockout and other probes of single-particle structure. It is also an interesting example where beam contamination was harnessed as a useful feature.

3.2. ISS — the ISOLDE Solenoidal Spectrometer at CERN

In 2018, the first two ISS experiments were performed using a 4-T magnet [17] and the HELIOS on-axis array. The ^{28}Mg(d, p) reaction at 9.47 MeV/u was performed with 10^6 pps to study single-particle states and test shell-model calculations on the border of the *island of inversion* where a change in nuclear shape occurs. The results highlighted the role of the geometry of the binding potential on the behaviour of orbitals close to the threshold [18]. A second run established excited states in ^{207}Hg using a 5×10^5-pps ^{206}Hg beam at 7.4 MeV/u in a first step in understanding single-particle structure in a region important for the astrophysical r-process [19].

Since 2021, ISS has operated with a double-sided Si strip array, initially commissioned with a stable ^{22}Ne beam; a plot of proton energy *versus* position is shown in Fig. 4 (a). The use of double-sided detectors makes it possible to correct for the non-linearity due to the finite array radius by measuring the position of the ions across the width of the detector, in addition to the measurement along z [20]; this algorithm will be implemented at a later date.

A variety of (d, p) studies have since been undertaken with ISS during two campaigns in 2021 and 2022. These include a study to extend measurements into the *island of inversion* with a ^{30}Mg beam. Single-particle strength along $N = 126$ has been probed in the ^{212}Rn(d, p) reaction. A ^{61}Zn beam was used to populate states using (d, p) whose mirror states in ^{62}Ga are relevant to a key rp-process step. Very recently, (d, p) reactions have been studied with the ^{11}Be, ^{27}Na, ^{110}Sn, ^{68}Ni, and ^{92}Kr beams to address a number of key topical questions in nuclear structure. Figure 4 shows the quality of some of the data obtained in preliminary analyses with Q-value resolutions of around 140 keV so far.

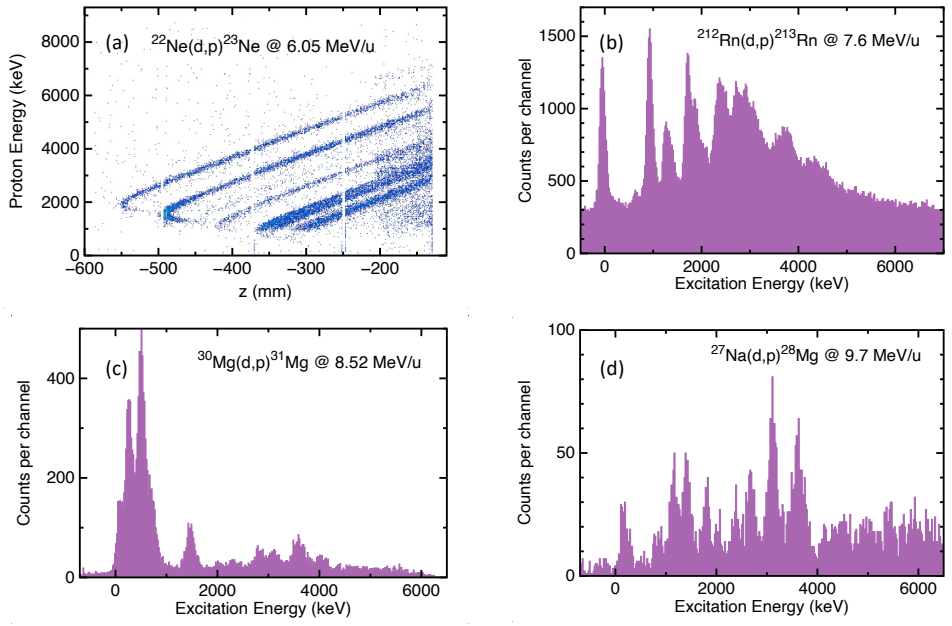

Fig. 4. (a) Data from the ISS commissioning reaction, ^{22}Ne(d, p). (b) Preliminary spectrum for the ^{212}Rn(d, p) reaction. The high background here arises from the α decay of scattered beam particles which will be removed in a time-random subtraction. (c) Preliminary spectrum from the ^{30}Mg(d, p) reaction. (d) Spectrum from the ^{27}Na(d, p) reaction using a partial data set.

3.3. SOLARIS — the solenoidal spectrometer at FRIB

A 4-T magnet of the same type as ISS was secured for SOLARIS [21] to be used with reaccelerated FRIB beams, as well as provide a field for the AT-TPC active target. Early experiments in 2021 employed the HELIOS detector system with beams of long-lived radioisotopes.

The ^{32}Si(d,p) reaction was used to investigate the trends in $2p$ spin-orbit partners, which here are relatively immune to tensor-driven shifts as protons are filling the $2s_{1/2}$ orbital. Experiments were also performed using the ^{10}Be(d,p) and ^{10}Be(t,p) reactions to address the lack of a detailed understanding of the interplay of *psd* orbitals near ^{12}Be. In the latter case, although the tritium content in the target is low and statistics limited, measurements in coincidence with the recoiling nuclei ensured almost background-free spectra shown in Fig. 5. There is a very rich programme of physics planned with intense radioactive-ion beams delivered by FRIB.

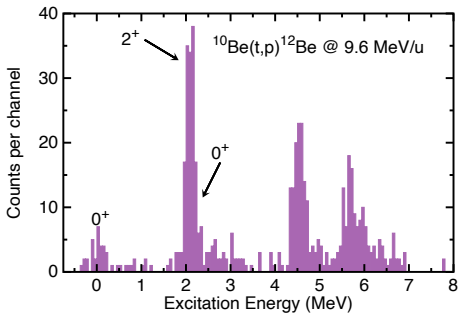

Fig. 5. Preliminary Q-value spectrum for the ^{10}Be(t,p) reaction at 9.6 MeV/u.

4. Conclusion and future plans

The simple and elegant method provided by a solenoidal spectrometer is now a well-established technique as the prolific record of scientific output from HELIOS illustrates. It is a method to complement others available for nuclear reactions with exotic beams.

The operation of the first such device used at an ISOL facility, ISS, is proceeding well and campaigns are planned to measure forward-going reactions. Following a successful test with a ^{238}U beam with HELIOS, studies of (d,p)-induced fission in nuclides away from stability are also planned. The construction of a dedicated dual array for SOLARIS to measure simultaneously in backward and forward hemispheres will harness the intense beams available from FRIB. Both SOLARIS and ISS magnets are used to provide fields for the AT-TPC and SPECMAT active targets that complement the

solenoidal spectrometers; an upgrade to ISS hopes to combine the advantages of an active target with the solenoidal method to produce a hybrid spectrometer.

The author would like to thank B.P. Kay, D.K. Sharp, L.P. Gaffney, and a very large number of collaborators who contributed to the experiments mentioned here. HELIOS is funded by the U.S. DOE Office of Science, Office of Nuclear Physics, under contract No. DE-AC02-06CH11357. SOLARIS is funded by the U.S. DOE Office of Science under the FRIB Cooperative Agreement DE-SC0000661. ISS is funded by the UK STFC, the EU Seventh Framework Programme ERC grant No. 617156, the Research Foundation Flanders, and EU Horizon Europe R&I programme under grant No. 101057511

REFERENCES

[1] J.R. Oppenheimer, M. Phillips, *Phys. Rev.* **48**, 500 (1935).
[2] R. Serber, *Phys. Rev.* **72**, 1008 (1947).
[3] H.B. Burrows, W.M. Gibson, J. Rotblat, *Phys. Rev.* **80**, 1095 (1950).
[4] S.T. Butler, *Phys. Rev.* **80**, 1095 (1950).
[5] J.R. Holt, C.T. Young, *Proc. Phys. Soc. A* **63**, 833 (1950).
[6] G. Satchler, «Introduction to Nuclear Reactions», *Wiley*, 1980.
[7] N.K. Glendenning, «Direct Nuclear Reactions», *World Scientific*, 2004.
[8] I.J. Thompson, F.M. Nunes, «Nuclear Reactions for Astrophysics», *Cambridge University Press*, 2009.
[9] K. Wimmer, *J. Phys. G: Nucl. Part. Phys.* **45**, 033002 (2018).
[10] As examples: C. Berner *et al.*, *Nucl. Instrum. Methods Phys. Res. A* **987**, 164827 (2021); M. Assié *et al.*, *Nucl. Instrum. Methods Phys. Res. A* **1014**, 165743 (2021), and `https://orruba.org`
[11] J.P. Schiffer, in: «Proceedings of the Workshop on Experimental Equipment for an Advanced ISOL Facility», *Lawrence Berkeley National Laboratory*, Berkeley, CA, USA 22–25 July, 1998, p. 667 (LBNL-42138).
[12] A.H. Wuosmaa *et al.*, *Nucl. Instrum. Methods Phys. Res. A* **580**, 1290 (2007).
[13] J.C. Lighthall *et al.*, *Nucl. Instrum. Methods Phys. Res. A* **622**, 97 (2010).
[14] `https://www.phy.anl.gov/atlas/helios/publication_list.html`
[15] B.P. Kay *et al.*, *Phys. Rev. Lett.* **129**, 152501 (2022).
[16] J.A. Tostevin, A. Gade, *Phys. Rev. C* **90**, 057602 (2014).
[17] `https://isolde-solenoidal-spectrometer.web.cern.ch`
[18] P.T. MacGregor *et al.*, *Phys. Rev. C* **104**, L051301 (2021).
[19] T.L. Tang *et al.*, *Phys. Rev. Lett.* **124**, 062502 (2020).
[20] P.A. Butler, private communication.
[21] `https://www.anl.gov/phy/solaris`